PHYSICAL REVIEW D **95,** 123509 (2017)

Reconstruction of the Scalar Field Potential in Inflationary Models with a Gauss-Bonnet term

Seoktae Koh,[1,*] Bum-Hoon Lee,[2,†] and Gansukh Tumurtushaa[2,3,‡]

[1]*Department of Science Education, Jeju National University, Jeju 63243, Korea*
[2]*Center for Quantum Spacetime, Sogang University, Seoul 121-742, Korea*
Department of Physics, Sogang University, Seoul 121-742, Korea
[3]*Center for Theoretical Physics of the Universe, Institute for Basic Science (IBS), Daejeon 34051, Korea*

(Received 6 March 2017; published 8 June 2017)

We consider inflationary models with a Gauss-Bonnet term to reconstruct the scalar-field potentials and the Gauss-Bonnet coupling functions. Both expressions are derived from the observationally favored configurations of n_s and r. Our result implies that, for the reconstructed potentials and coupling functions, the blue tilt of inflationary tensor fluctuations can be realized. To achieve a blue tilt for the inflationary tensor fluctuations, a scalar field must climb up its potential before rolling down. We further investigate the properties of propagation of the perturbation modes in Friedmann-Robertson-Walker spacetime. For the reconstructed configurations that give rise to the blue tilt for the inflationary tensor fluctuations, we show that the ghosts and instabilities are absent with the superluminal propagation speeds for the scalar perturbation modes, whereas the propagation speeds of the tensor perturbations are subluminal.

DOI: 10.1103/PhysRevD.95.123509

I. INTRODUCTION

Cosmological observations including the cosmic microwave background (CMB) anisotropies by the WMAP [1] and Planck collaborations [2,3] have the prospect of providing precise constraints on models for the origin of the large-scale structure, among which inflation [4] is currently the leading candidate. Although there exist hundreds of different inflationary models in the market at present [5], the inflationary scenario remains successful at explaining the current observations. In spite of its successes, however, the simplest models of chaotic inflation are now observationally disfavored due to its prediction of the large tensor-to-scalar ratio [3]. Instead, extended models of inflation involving modified theories of gravity are now attracting more considerable interest [6,7].

If we consider the early Universe approaching the Planck scale, it is widely believed that quantum gravity would play an important role. Since we do not have any complete theory of quantum gravity yet, we consider Einstein gravity with some modifications as the effective theory of ultimate quantum gravity. One such modification is to consider the Gauss-Bonnet term, which appears naturally in the low-energy effective theory of string theory and in renormalizing the stress tensor in curved spacetime. Previously, in Refs. [8–12], inflationary models with a Gauss-Bonnet term were studied, and as the theories beyond standard single-field slow-roll inflation, their predictions were found to be consistent with the observation. Hence, if certain forms of the potentials and the coupling functions are given, one can compute the observable quantities and provide constrains on those quantities in light of observations.

On the other hand, if a particular set of observations with some accuracy is given, one can attempt the task of reconstructing the inflaton potential, either numerically or analytically, from the observational data [2,3]. Motivated by this interest, reconstruction methods of the scalar-field potentials in inflationary models without a Gauss-Bonnet term are investigated [13–16]. As such, in this paper, we attempt the inverse problem of reconstructing the inflaton potentials in inflationary models with the Gauss-Bonnet term analytically by using observationally favored configurations of the observable quantities. In this sense, our work is an extension of the work that was previously done in Ref. [15]. Moreover, we apply the authors' approach to the inflationary models with a Gauss-Bonnet term that is nonminimally coupled to a dynamical scalar field.

An interesting feature of the inflationary models with a Gauss-Bonnet term is the violation of the consistency relation ($r = -8n_t$). In the conventional inflation models, where the scalar field is minimally coupled to gravity, the Hubble rate H monotonically decreases ($\dot{H} < 0$), and hence the first slow-roll parameter is positive ($\epsilon > 0$). Thus, it is implied that the spectral index of the primordial tensor fluctuation ($n_t = -2\epsilon$) is always negative. Therefore, the spectrum of the tensor modes is always red tilted. Although the present observations cannot determine the tilt of the tensor spectral index, it is interesting to investigate the blue-tilted spectrum of the tensor fluctuations in inflationary cosmology from the perspective of theoretical interpretations [17].

*kundol.koh@jejunu.ac.kr
†bhl@sogang.ac.kr
‡gansuh@sogang.ac.kr

If the blue-tilted spectrum is realized, in order to test the cosmological viability and the compatibility with the observational data, one needs to check the stabilities of the perturbation modes. Thus, by applying the criterion previously discussed in Refs. [18–21], we investigate the stability conditions in the inflationary models with a Gauss-Bonnet term by using the reconstructed configurations of the potential and the coupling functions. As a result, we show that both the ghosts and the instabilities are absent in our model. We further find that the propagation speeds for the scalar perturbations are superluminal, whereas those of the tensor perturbations are subluminal.

This paper is organized as follows. In Sec. II, we briefly present the main feature of the model studied in Ref. [12] together with the procedure for reconstructing the inflaton potential. In Sec. III, several examples of the inflaton potential, as well as the Gauss-Bonnet coupling functions, are reconstructed from the observationally favored configurations of n_s and r. Our result implies that, as is discussed in Sec. IV, the blue tilt for inflationary tensor fluctuations can be achieved. Section V is devoted to the analysis of the cosmological perturbations in inflation with a Gauss-Bonnet term, namely, propagation of the perturbation in Friedmann-Robertson-Walker (FRW) spacetime. We summarize our result in Sec. VI. The unit of $\kappa^2 = 8\pi G = M_{\rm pl}^{-2}$ is used throughout this paper.

II. COSMOLOGICAL PERTURBATIONS

The action that we consider is composed of the Einstein-Hilbert term and the canonical scalar field, which couples nonminimally to the Gauss-Bonnet term through the coupling function $\xi(\phi)$,

$$S = \int d^4x\sqrt{-g}\left[\frac{1}{2\kappa^2}R - \frac{1}{2}g^{\mu\nu}\partial_\mu\phi\partial_\nu\phi - V(\phi) - \frac{1}{2}\xi(\phi)R^2_{\rm GB}\right], \tag{1}$$

where $R^2_{\rm GB} = R_{\mu\nu\rho\sigma}R^{\mu\nu\rho\sigma} - 4R_{\mu\nu}R^{\mu\nu} + R^2$ is the Gauss-Bonnet term. The Gauss-Bonnet coupling $\xi(\phi)$ is required to be a function of a scalar field in order to give nontrivial effects on the background dynamics. In a FRW universe with a scale factor a and with an arbitrary constant curvature K,

$$ds^2 = -dt^2 + a^2\left(\frac{dr^2}{1-Kr^2} + r^2d\Omega^2\right), \tag{2}$$

the background dynamics of this system yields the Einstein and the field equations

$$H^2 = \frac{\kappa^2}{3}\left[\frac{1}{2}\dot\phi^2 + V - \frac{3K}{\kappa^2a^2} + 12\dot\xi H\left(H^2 + \frac{K}{a^2}\right)\right], \tag{3}$$

$$\dot H = -\frac{\kappa^2}{2}\left[\dot\phi^2 - \frac{2K}{\kappa^2a^2} - 4\ddot\xi\left(H^2 + \frac{K}{a^2}\right) - 4\dot\xi H\left(2\dot H - H^2 - \frac{3K}{a^2}\right)\right], \tag{4}$$

$$\ddot\phi + 3H\dot\phi + V_\phi + 12\xi_\phi\left(H^2 + \frac{K}{a^2}\right)(\dot H + H^2) = 0, \tag{5}$$

where a dot represents a derivative with respect to the cosmic time t, $H \equiv \dot a/a$ denotes the Hubble parameter, $V_\phi = \partial V/\partial\phi$, and $\xi_\phi = \partial\xi/\partial\phi$. Since ξ is a function of ϕ, $\dot\xi$ implies $\dot\xi = \xi_\phi\dot\phi$. If ξ is a constant, the background dynamics would not be influenced by the Gauss-Bonnet term because it is known that the Gauss-Bonnet in four-dimensional spacetime is a topological term.

In this work, we consider the case in which a scalar field slowly rolls down to the minimum of the potential and the Gauss-Bonnet term is assumed to be a small correction to gravity. Hence, the following inequality must be satisfied [12]:

$$\dot\phi^2/2 \ll V, \quad \ddot\phi \ll 3H\dot\phi, \quad 4\dot\xi H \ll 1, \text{ and } \ddot\xi \ll \dot\xi H. \tag{6}$$

To reflect the slow-roll approximations above, we define the following slow-roll parameters:

$$\epsilon \equiv -\frac{\dot H}{H^2}, \quad \eta \equiv \frac{\ddot H}{H\dot H}, \quad \delta_1 \equiv 4\kappa^2\dot\xi H, \quad \delta_2 \equiv \frac{\ddot\xi}{\dot\xi H}. \tag{7}$$

Under Eq. (6), Eqs. (3)–(5) become for $K = 0$

$$H^2 \simeq \frac{\kappa^2}{3}V, \tag{8}$$

$$\dot H \simeq -\frac{\kappa^2}{2}(\dot\phi^2 + 4\dot\xi H^3), \tag{9}$$

$$3H\dot\phi + V_\phi + 12\xi_\phi H^4 \simeq 0. \tag{10}$$

We rewrite Eq. (7) in terms of the potential and the Gauss-Bonnet coupling function as

$$\epsilon = \frac{1}{2\kappa^2}\frac{V_\phi}{V}Q, \tag{11}$$

$$\eta = -\frac{1}{\kappa^2}\left(\frac{V_{\phi\phi}}{V_\phi}Q + Q_\phi\right), \tag{12}$$

$$\delta_1 = -\frac{4\kappa^2}{3}\xi_\phi VQ, \tag{13}$$

$$\delta_2 = -\frac{1}{\kappa^2}\left(\frac{\xi_{\phi\phi}}{\xi_\phi}Q + \frac{1}{2}\frac{V_\phi}{V}Q + Q_\phi\right), \tag{14}$$

where

$$Q \equiv \frac{V_\phi}{V} + \frac{4}{3}\kappa^4 \xi_\phi V. \tag{15}$$

Another key parameter in an inflationary scenario is the e-folding number, N, that measures the amount of inflationary expansion from a particular time t until the end of inflation t_e,

$$N = \int_t^{t_e} H dt \simeq \int_{\phi_e}^{\phi} \frac{\kappa^2}{Q} d\phi, \tag{16}$$

where $\phi_e = \phi(t_e)$ is the field value at the end of inflation. To give the standard reheating process, $N \simeq 50 \sim 60$ is assumed at the horizon crossing time, $k = aH$, where k is the comoving scale.

Let us consider following linearized perturbation metric in the comoving gauge in which $\delta\phi = 0$ [12],

$$ds^2 = a(\tau)^2[-d\tau^2 + \{(1-2\mathcal{R})\delta_{ij} + h_{ij}\}dx^i dx^j], \tag{17}$$

where $\mathcal{R}$ represents the curvature perturbation on the uniform field hypersurfaces and h_{ij} is the tensor perturbation that satisfies $h^i{}_i = 0 = h^i{}_{j,i}$. At the linear order in perturbation theory, the Fourier modes of the curvature and tensor perturbations satisfy [11,12,22]

$$v_A'' + \left(c_A^2 k^2 - \frac{z_A''}{z_A}\right) v_A = 0, \tag{18}$$

where $A = \{s, t\}$ represents the scalar and tensor perturbations, respectively; a prime denotes a derivative with respect to the conformal time $\tau = \int a^{-1} dt$; and

$$\begin{aligned} c_s^2 &\equiv 1 + \frac{2(\dot{H} - \kappa^2\dot{\xi}H(H^2 + 4\dot{H}) + \kappa^2\ddot{\xi}H^2)\Delta^2}{\kappa^2\dot{\phi}^2 + 6\kappa^2\dot{\xi}H^3\Delta}, \\ c_t^2 &\equiv 1 - \frac{4\kappa^2(\ddot{\xi} - \dot{\xi}H)}{1 - 4\kappa^2\dot{\xi}H} \end{aligned} \tag{19}$$

and

$$\begin{aligned} z_s &\equiv \sqrt{\frac{a^2(\dot{\phi}^2 + 6\dot{\xi}H^3\Delta)}{H^2(1-\frac{1}{2}\Delta)^2}}, \\ z_t &\equiv \sqrt{\frac{a^2}{\kappa^2}(1 - 4\kappa^2\dot{\xi}H)}, \end{aligned} \tag{20}$$

with $\Delta = 4\kappa^2\dot{\xi}H/(1 - 4\kappa^2\dot{\xi}H)$. By using the definitions of the slow-roll parameters (6), one can write Eqs. (19)–(20) in terms of the slow-roll parameters [11,12,22],

$$\begin{aligned} c_s^2 &= 1 - \frac{(4\epsilon + \delta_1(1 - 4\epsilon - \delta_2))\Delta^2}{4\epsilon - 2\delta_1 - 2\delta_1(2\epsilon - \delta_2) + 3\delta_1\Delta}, \\ c_t^2 &= 1 + \frac{\delta_1(1-\delta_2)}{1-\delta_1}, \end{aligned} \tag{21}$$

$$\begin{aligned} z_s &= \sqrt{\frac{a^2}{\kappa^2}\frac{2\epsilon - \delta_1(1 + 2\epsilon - \delta_2) + \frac{3}{2}\delta_1\Delta}{(1-\frac{1}{2}\Delta)^2}}, \\ z_t &= \sqrt{\frac{a^2}{\kappa^2}(1-\delta_1)}, \end{aligned} \tag{22}$$

with $\Delta = \delta_1/(1-\delta_1)$. Here, it is worth it to note that the terms under square root in Eq. (22) must be positive; otherwise, a ghost would appear in the theory [18–21]. We will discuss the details of this in Sec. V. If one keeps the leading order of the slow-roll parameters in z_A''/z_A using Eq. (22), Eq. (18) becomes

$$v_A'' + \left(c_A^2 k^2 - \frac{\nu_A^2 - 1/4}{\tau^2}\right) v_A = 0, \tag{23}$$

where the parameters are given up to leading order in the slow-roll parameters [12]

$$\nu_s \simeq \frac{3}{2} + \epsilon + \frac{2\epsilon(2\epsilon + \eta) - \delta_1(\delta_2 - \epsilon)}{4\epsilon - 2\delta_1}, \tag{24}$$

$$\nu_t \simeq \frac{3}{2} + \epsilon. \tag{25}$$

The general solutions of Eq. (23) can be obtained as a linear combination of Hankel functions if the slow-roll parameters are assumed to be constants,

$$v_A = \frac{\sqrt{\pi|\tau|}}{2}[c_1^A(k) H_{\nu_A}^{(1)}(c_A k|\tau|) + c_2^A(k) H_{\nu_A}^{(2)}(c_A k|\tau|)], \tag{26}$$

where $H_\nu^{(i)}(i = 1, 2)$ are the first- and second-kind Hankel functions. $c_i^A(i = 1, 2)$ are the coefficients which are determined from the initial conditions and satisfy the normalization conditions

$$|c_2^A|^2 - |c_1^A|^2 = 1. \tag{27}$$

If we adopt the Bunch-Davies vacuum which is defined in the asymptotic past, by taking the positive frequency mode solutions, one can obtain $c_1^A = e^{i(\nu_A + \frac{1}{2})\frac{\pi}{2}}$ and $c_2^A = 0$.[1] The exact solution of Eq. (26) becomes

$$v_A = \frac{\sqrt{\pi|\tau|}}{2} e^{i(\nu_A + \frac{1}{2})\frac{\pi}{2}} H_{\nu_A}^{(1)}(c_A k|\tau|). \tag{28}$$

[1]Details can be found in Ref. [12].

The power spectra of the scalar and tensor modes are calculated as

$$\mathcal{P}_s \simeq \frac{\csc^2\nu_s\pi}{\pi\mathcal{D}_s^2\Gamma^2(1-\nu_s)}\frac{1}{c_s^3|\tau|^2a^2}\left(\frac{c_sk|\tau|}{2}\right)^{3-2\nu_s}, \quad (29)$$

$$\mathcal{P}_t \simeq 8\frac{\csc^2\nu_t\pi}{\pi\mathcal{D}_t^2\Gamma^2(1-\nu_t)}\frac{1}{c_t^3|\tau|^2a^2}\left(\frac{c_tk|\tau|}{2}\right)^{3-2\nu_t}, \quad (30)$$

where $\mathcal{D}_A \equiv z_A/a^2$. The spectral indices of the scalar and tensor perturbation modes and the tensor-to-scalar ratio are obtained in Ref. [12] as

$$n_s - 1 \approx -2\epsilon - \frac{2\epsilon(2\epsilon+\eta)-\delta_1(\delta_2-\epsilon)}{2\epsilon-\delta_1}, \quad (31)$$

$$n_t \approx -2\epsilon, \quad (32)$$

$$r \approx 8(2\epsilon-\delta_1). \quad (33)$$

If the potential and the Gauss-Bonnet coupling function are given, the observable quantities can be obtained up to leading order in terms of the slow-roll parameters. Subsequently, by using Eqs. (31)–(33) for the given potentials and the Gauss-Bonnet coupling functions, one can check the consistency of the models by the observational data.

In this work, however, we are interested in the inverse problem of reconstructing the inflaton potentials $V(\phi)$ and the Gauss-Bonnet coupling functions $\xi(\phi)$ from the observational data [2,3]. To reconstruct $V(\phi)$ and $\xi(\phi)$, we start with Eqs. (31)–(33), where n_s and r can be expressed as functions of N. By using Eq. (16), however, we can write them as a function of ϕ. Since the observable quantities can be expressed as the functions of N [1–3], it is convenient to rewrite the slow-roll parameters in terms of N as

$$\epsilon = \frac{1}{2}\frac{V_N}{V}, \quad (34)$$

$$\eta = -\frac{V_{NN}}{V_N} = -2\epsilon - \frac{d\ln\epsilon}{dN}, \quad (35)$$

$$\delta_1 = -\frac{4}{3}\kappa^4\xi_N V, \quad (36)$$

$$\delta_2 = -\frac{\xi_{NN}}{\xi_N} - \frac{1}{2}\frac{V_N}{V} = \epsilon - \frac{d\ln\delta_1}{dN}, \quad (37)$$

where $V_N = \partial V/\partial N$ and $\xi_N = \partial\xi/\partial N$. By using Eqs. (34)–(37), we rewrite Eqs. (31)–(33) as

$$n_s(N) - 1 = \left[\ln\left(\frac{V_N}{V^2} + \frac{4}{3}\kappa^4\xi_N\right)\right]_{,N}, \quad (38)$$

$$r(N) = 8\left(\frac{V_N}{V} + \frac{4}{3}\kappa^4\xi_N V\right) = 8Q^{(N)}, \quad (39)$$

$$n_t(N) = -\frac{V_N}{V}, \quad (40)$$

where $[\ldots]_{,N}$ represents a derivative with respect to the e-folding number N. From Eqs. (38)–(39), we find

$$V(N) = \frac{1}{8c_1}r(N)e^{-\int[n_s(N)-1]dN}, \quad (41)$$

and by substituting Eq. (41) into Eq. (39),

$$\xi(N) = \frac{3}{4\kappa^4}\left[\frac{1}{V(N)} + \int\frac{r(N)}{8V(N)}dN + c_2\right], \quad (42)$$

where c_1 and c_2 are the integration constants. If the particular form of $n_s - 1$ and r are given, therefore, one can reconstruct the scalar-field potential and the Gauss-Bonnet coupling functions. Using Eq. (16) together with Eq. (39), one also can find the relation between the number of e-folding N and the scalar field ϕ as

$$\int_{\phi_e}^{\phi} d\phi = \int\sqrt{\frac{r(N)}{8\kappa^2}}dN. \quad (43)$$

In the following sections, we apply this approach to the particular models and investigate further properties of those models.

III. RECONSTRUCTING THE POTENTIAL AND THE COUPLING FUNCTIONS

There are hundreds of inflationary models in the market today that show good fit with the observational data [2,3,5]. Therefore, the slow-roll formalism for inflationary models with a Gauss-Bonnet term is not unfamiliar and was previously studied with the particular potentials and the coupling functions [9–12]. Although theoretical predictions of those models are, in some parameter range, compatible with the observational data, the observable quantities are obtained differently in each model; hence, it is hard to figure out the best inflation model even when the model parameters accurately fit with the data. In this section, therefore, we reconstruct the inflaton potentials, as well as the Gauss-Bonnet coupling functions, that are in good agreement with the latest observational data by using the expressions for n_s and r. We consider

$$n_s - 1 = -\frac{\beta}{N+\alpha}, \quad (44)$$

$$r = \frac{q}{N^p + \gamma N + \alpha}, \quad (45)$$

where β, γ, p, and q parameters are arbitrary integers, while α is also an arbitrary constant but not required to be an integer. These model parameters can be chosen in such a way that the relations in Eqs. (44)–(45) are consistent with the observations [2,3]. More importantly, Eqs. (44)–(45) cover most of standard inflation models, where the Gauss-Bonnet term is absent, discussed in Ref. [2,3], and the models with a Gauss-Bonnet term; for example, Ref. [11] must be recovered if $p = 1$ and $\gamma = 0$ in Eq. (45).

Previously in Refs. [14–16], an inverse problem of reconstructing the scalar-field potential was studied for the models without the Gauss-Bonnet term. If the Gauss-Bonnet term is present with the constant coupling in Eq. (1), however, the consequent result must be consistent with that of Ref. [15], where the authors use the same relation as Eq. (44) but $\alpha = 0$ is considered. This is so because the Gauss-Bonnet term is known as a topological term in four dimensions. Therefore, we will show that the scalar-field potential obtained in Ref. [15] can also be obtained in our model. We introduce nonzero α because its presence enables the n_s value to be best fit with data.

In the following two subsections, we employ with the different configurations of Eqs. (44)–(45) to reconstruct different potentials and coupling functions. In Secs. III A and III B 1, we aim to test our approach by reproducing the scalar-field potential that is obtained in Refs. [11,15]. Then, Sec. III B 2 is devoted to reconstructing a new type of potential and coupling functions that have not been considered before. Hence, without loss of generality, we set $\gamma = 1$ in Sec. III A and $\gamma = 0$ in Sec. III B.

A. Models with $\gamma = 1$

To be consistent with Ref. [15], we set $\beta = p = 2$ and $q = 8$, for which Eqs. (44)–(45) become

$$n_s - 1 = -\frac{2}{N+\alpha}, \tag{46}$$

$$r = \frac{8}{N^2+N+\alpha}. \tag{47}$$

From Eqs. (41)–(42), we obtain

$$V(N) = \frac{(N+\alpha)^2}{c_1(N^2+N+\alpha)}, \tag{48}$$

$$\xi(N) = -\frac{3}{4\kappa^4}\left[-\frac{N^2}{(N+\alpha)^2}c_1 + c_2\right]. \tag{49}$$

By using Eq. (43), we obtain N as the functions of ϕ,

$$N = \frac{1}{4}[(1-4\alpha)e^{-\kappa(\phi-C)} + e^{\kappa(\phi-C)} - 2], \tag{50}$$

where C is an integration constant and is responsible for the shift of ϕ. Now, we can rewrite both the potential and the coupling functions in terms of the scalar field,

$$V(\phi) = \frac{(e^{\kappa(\phi-C)}-1)^2(4\alpha + e^{\kappa(\phi-C)}-1)^2}{c_1(4\alpha + e^{2\kappa(\phi-C)}-1)^2}, \tag{51}$$

$$\xi(\phi) = \frac{3}{4\kappa^4}\left[\frac{(1-2e^{\kappa(C-\phi)}-(4\alpha-1)e^{2\kappa(C-\phi)})^2}{(1-e^{-\kappa(\phi-C)})^2(1+(4\alpha-1)e^{-\kappa(\phi-C)})^2}c_1 - c_2\right]. \tag{52}$$

In the $\alpha \to 0$ limit, the leading-order contribution gives

$$V(\phi) = c_1 \tanh^2\left(\frac{1}{2}\kappa(\phi - C)\right),$$
$$\xi(\phi) = \frac{3}{4\kappa^4}(c_1 - c_2). \tag{53}$$

The Gauss-Bonnet coupling function in Eq. (53) becomes zero if $c_1 = c_2$ or constant otherwise. In either case, the Gauss-Bonnet term does not give any effects on the background evolution in four dimensions. Therefore, the background evolution in our model reduces to Einstein gravity. And our result in Eq. (53) successfully reproduces the potentials obtained in Refs. [15,23].

B. Models with $\gamma = 0$

In this subsection, for simplicity, we consider the $\gamma = 0$ case. If $\gamma = 0$, Eqs. (44)–(45) become

$$n_s(N) - 1 = -\frac{\beta}{N+\alpha}, \tag{54}$$

$$r(N) = \frac{q}{N^p+\alpha}. \tag{55}$$

After substituting Eqs. (54)–(55) into Eq. (42), we obtain

$$\xi(N) = \frac{3}{4\kappa^4}\left[\left(\frac{8}{q}\frac{N^p+\alpha}{(N+\alpha)^\beta} + \frac{(N+\alpha)^{1-\beta}}{1-\beta}\right)c_1 + c_2\right], \tag{56}$$

where $\beta \neq 1$ is assumed.[2] The scalar-field potential can also be obtained with the help of Eq. (41) as

$$V(N) = \frac{q}{8c_1}\frac{(N+\alpha)^\beta}{N^p+\alpha}. \tag{57}$$

[2]The $\beta = 1$ case is not considered in this paper. If $\beta = 1$, from Eq. (54), the number of e-folds needs to be $N \sim 30 - \alpha$ in order to be consistent with the observational value of $n_s \sim 0.9655 \pm 0.0062$ [3]. On the other hand, $N \simeq 50 \sim 60$ is needed for inflation; hence, α must take negative values between $-30 \leq \alpha \leq -20$, which later conflicts with Eq. (58) where $\alpha > 0$ is necessary. For the $\beta \neq 1$ case, however, no such contradictions occur.

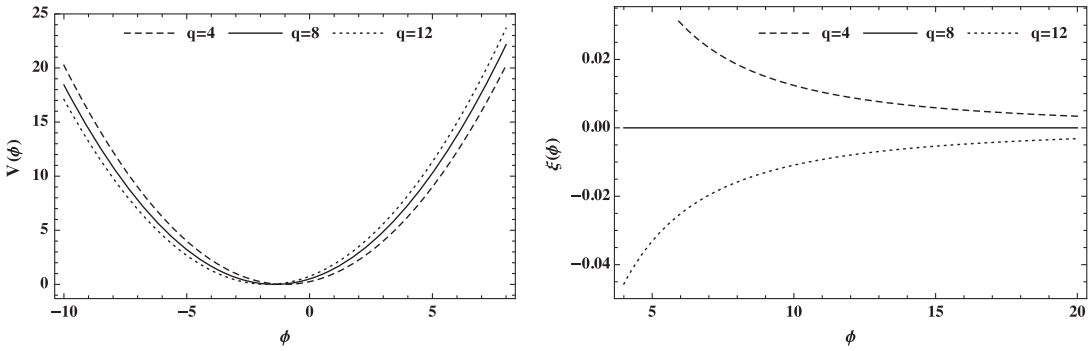

FIG. 1. Numerical plot of Eqs. (63) and (64) with $c_1 = 1$, $c_2 = 0$, $\kappa^2 = 1$, and $n = 2$.

Equation (43) gives

$$\phi - \phi_e = N\sqrt{\frac{q}{8\kappa^2\alpha^2}}F_1\left(\frac{1}{2},\frac{1}{p};1+\frac{1}{p};-\frac{N^p}{\alpha}\right), \tag{58}$$

where $\alpha > 0$ is necessary because the positive q is favored by the observations [2,3]. It is often assumed for large-field inflation that the field value at the end of inflation is negligible compared to that of the beginning of inflation, $\phi_e \ll \phi$. Therefore, from now and throughout the rest of this paper, we will ignore ϕ_e by assuming the large-field inflation model in mind. It is difficult to solve Eq. (57) for N for $p \geq 3$; hence, for simplicity, we will consider only the $p = 1$ and $p = 2$ cases, respectively, in the following two subsections.

1. p = 1 case

If $p = 1$ in Eq. (55), the corresponding n_s and r relations look the same as those obtained in Ref. [11]. Thus, as the result, the monomial potentials and the inverse monomial coupling functions are expected. When $p = 1$, we obtain from Eq. (58)

$$N = \left(\frac{2\kappa^2}{q}\phi^2 + \sqrt{\frac{8\alpha}{q}}\kappa\phi\right), \tag{59}$$

where $q \neq 0$ and Eqs. (56)–(57) give

$$V(\phi) = \frac{q}{8c_1}\left(\alpha + \frac{2}{q}\kappa^2\phi^2 + \sqrt{\frac{8\alpha}{q}}\kappa\phi\right)^{\beta-1}, \tag{60}$$

$$\xi(\phi) = \frac{3}{4\kappa^4}\left[\frac{q+8(1-\beta)}{q(1-\beta)}\left(\alpha + \frac{2}{q}\kappa^2\phi^2 + \sqrt{\frac{8\alpha}{q}}\kappa\phi\right)^{1-\beta}c_1 + c_2\right]. \tag{61}$$

To be more consistent with Ref. [11], it is worth it to express α and β in terms of the new parameter, n, as follows:

$$\alpha = \frac{n}{4}, \qquad \beta = \frac{n+2}{2}. \tag{62}$$

Equations (60)–(61) can be rewritten as

$$V(\phi) = \frac{q}{8c_1}\left(\frac{n}{4} + \frac{2}{q}\kappa^2\phi^2 + \sqrt{\frac{2n}{q}}\kappa\phi\right)^{\frac{n}{2}}, \tag{63}$$

$$\xi(\phi) = \frac{3}{4\kappa^4}\left[\frac{8n-2q}{nq}\left(\frac{n}{4} + \frac{2}{q}\kappa^2\phi^2 + \sqrt{\frac{2n}{q}}\kappa\phi\right)^{-\frac{n}{2}}c_1 + c_2\right]. \tag{64}$$

From Eq. (64), one can see $\xi(\phi) = 0$ for every $q = 4n$ if $c_2 = 0$ or $\xi(\phi) = \text{const.}$ for every $q = 4n$ if $c_2 \neq 0$. This can also be seen in Fig. 1 where we plot Eqs. (63) and (64) with $n = 2$. In either case, the background evolution would be described by Einstein gravity with a dynamical scalar field. In Fig. 1, the potential takes its minimum value at $\phi_{\min} = 0$ for $\alpha = 0$, and it shifts to $\phi_{\min} = -\sqrt{nq/(8\kappa^2)}$ if $\alpha \neq 0$ depending on n and q values. However, the scalar field can be rescaled such that the minimum stays at the origin. If $c_2 = 0$ in Eq. (64), the Gauss-Bonnet coupling functions hold the inverse relation to monomial potentials, $\xi(\phi) \sim 1/V(\phi)$.

2. p = 2 case

For the $p = 2$ case, we obtain from Eq. (58)

$$N = \sqrt{\alpha}\sinh\left(\sqrt{\frac{8}{q}}\kappa\phi\right), \tag{65}$$

where $\alpha > 0$ and $q > 0$ are assumed. By substituting Eq. (65) into Eqs. (56)–(57), we get

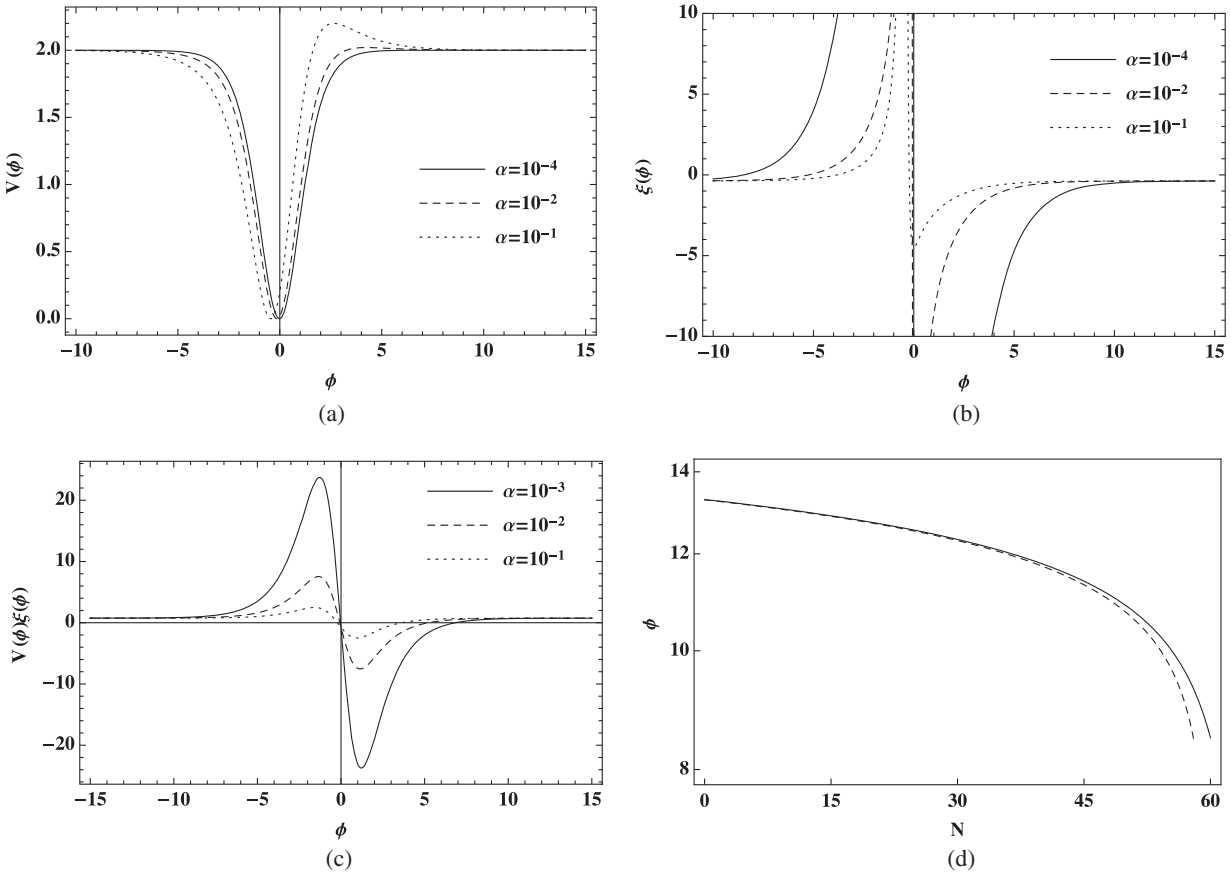

FIG. 2. We plot Eqs. (66) and (67) in the first row. The relation between the potential and the coupling function is plotted in Fig. 2(c). Figure 2(d) shows the comparison between the numerical solution (solid) of Eqs. (3)–(5) and the slow-roll solution (dashed) obtained in Eq. (68).

$$V(\phi) = \frac{q}{8c_1\alpha}\,\mathrm{sech}^2\left(\sqrt{\frac{8}{q}}\kappa\phi\right)\left[\alpha + \sqrt{\alpha}\sinh\left(\sqrt{\frac{8}{q}}\kappa\phi\right)\right]^{\beta}, \tag{66}$$

$$\xi(\phi) = \frac{3}{4\kappa^4}\left[\frac{q\left(\alpha + \sqrt{\alpha}\sinh\left(\sqrt{\frac{8}{q}}\kappa\phi\right)\right) + 8(1-\beta)\alpha\cosh^2\left(\sqrt{\frac{8}{q}}\kappa\phi\right)}{q(1-\beta)\left(\alpha + \sqrt{\alpha}\sinh\left(\sqrt{\frac{8}{q}}\kappa\phi\right)\right)^{\beta}}c_1 + c_2\right], \tag{67}$$

where $\beta \neq 1$. We plot Eqs. (66)–(67) in Fig. 2 by setting $c_1 = 1$, $c_2 = 0$, $\kappa^2 = 1$, $\alpha = 10^{-4}$, $\beta = 2$, $q = 16$, $K = 0$, $\phi_0 = 13.28$, $\dot{\phi}_0 = 0$, and $C = 8.4 \times 10^3$. The overall shape of the reconstructed potential is, in Fig. 2(a), similar to that of a "T model" studied in Ref. [23] with a small bump on the side which eventually disappears for $\alpha = 0$. The existence of such a bump in the potential may be important in achieving the blue-tilted spectrum for inflationary tensor fluctuations as was discussed in Ref. [8]. We will discuss such possibilities of the blue-tilted spectrum for inflationary tensor modes in the next section.

Previously, in the $p = 1$ case, we were able to see an inverse relation between the potentials and the Gauss-Bonnet coupling functions if $c_2 = 0$. In the $p = 2$ case, on the other hand, such an inverse relation can be hold in an infinitely large region $-\infty < \phi < \infty$, everywhere except a finite interval $O(5)$ near $\phi = 0$ in Fig. 2(c). By substituting Eqs. (66) and (67) with $\beta = 2$ into Eqs. (8)–(10), we obtain the slow-roll solution for the scalar field

$$\phi(N) = -\sqrt{\frac{q}{8\kappa^2}}\,\mathrm{arcsinh}\left(\frac{N}{\sqrt{\alpha}} - \sqrt{\frac{8\kappa^2}{q}}C\right), \tag{68}$$

where C is an arbitrary constant. We compare the slow-roll solution obtained in Eq. (68) with the numerical solution of Eqs. (3)–(5) in Fig. 2(d). It can be seen in Fig. 2(d) that the slow-roll solution fits well with the numerical solution during inflationary period. In the $\alpha \to 0$ limit, Eqs. (66) and (67) can be reduced to

$$V(\phi) \sim \tanh^2\left(\sqrt{\frac{8}{q}}\kappa\phi\right),$$
$$\xi(\phi) \sim -\frac{3c_1}{4\sqrt{\alpha}\kappa^4}\,\mathrm{csch}\left(\sqrt{\frac{8}{q}}\kappa\phi\right). \tag{69}$$

In Fig. 3, we compare the predictions of the spectral index and tensor-to-scalar ratio for three different models; namely, the chaotic inflation with dilatonlike coupling [9]; the chaotic inflation with an inverse power-law coupling [11], which we also discussed in Sec. III B 1; and the inflation models with Eqs. (66)–(67). For the chaotic inflation with dilatonlike coupling, following Ref. [9], we use

$$V(\phi) = V_0\phi^n, \qquad \xi(\phi) = \xi_0 e^{-\lambda\phi} \tag{70}$$

in our comparison. From Eqs. (31) and (33), by using Eq. (70), we obtain the scalar spectral index and tensor-to-scalar ratio,

$$n_s - 1 = -\frac{1}{\phi^2}[n(n+2) + \tilde{\alpha}\lambda e^{-\lambda\phi}\phi^{n+1}(n - 2\lambda\phi)],$$
$$r = \frac{8}{\phi^2}(n - \tilde{\alpha}\lambda e^{-\lambda\phi}\phi^{n+1})^2, \tag{71}$$

where $\kappa^2 = 1$ is considered.[3] In Fig. 3, we numerically plot Eq. (71) with $n = 2$ and $\lambda = 0.29$ in green. Along the green line, from the yellow end point to the light-blue end point, the number of e-foldings is fixed to $N = 60$, while the $\tilde{\alpha}$ value varies between $0 \le \tilde{\alpha} \le 0.12$. We use Eqs. (54)–(55) as theoretical predictions for the remaining two models. In our numerical study, therefore, we use Eqs. (54)–(55) with $p = 1$ for the dashed line and $p = 2$ for the solid line along which the q value is fixed to $q = 8$. However, along the vertical red and dashed-blue lines where the number of e-folds is fixed to $N = 60$, the parameter q varies between $0 \le q \le 8$. In this slow-roll inflationary scenario with $p = 2$, the Gauss-Bonnet term slows down the evolution of the inflaton during inflation, which decreases the energy scale of the potential be to in agreement with the amplitude of scalar perturbations. Hence, the tensor-to-scalar ratio is suppressed. Compared to the chaotic inflation with dilaton-like coupling [9] and the chaotic inflation with an inverse power-law coupling [11], the reconstructed configurations in Eqs. (66)–(67) give rise to the observable quantities that are excellently consistent with the Planck constraints.

[3]To avoid confusion of the same notation, we use $\tilde{\alpha}$ instead of α, which was used in Ref. [9].

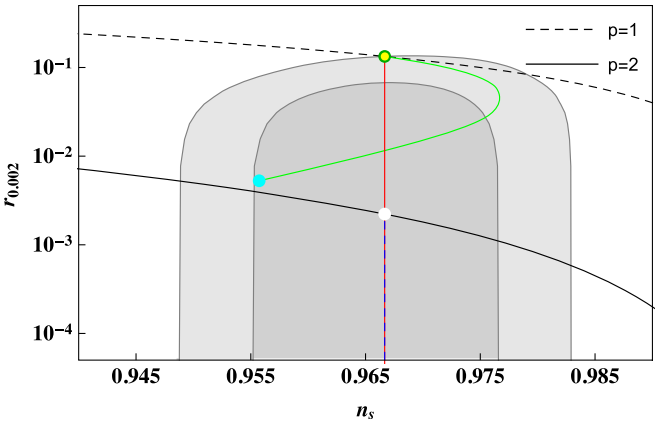

FIG. 3. Predicted n_s vs r in three different models; namely, the red line represents the model in Eqs. (63)–(64) with $n = 2$, the blue-dashed line corresponds to the model Eqs. (66)–(67) with $\alpha = 10^{-4}$, and the green line is for the model in Eq. (70) with $n = 2$ and $\lambda = 0.29$. The black dashed and solid lines indicate the $p = 1$ and $p = 2$ cases in Eq. (55), respectively. The contours show the 68% and 95% confidence levels from the Planck2015 TT + lowP. Here, we choose $N = 60$ for all end points. For the remaining parameters, we use the same numerical inputs as Fig. 2.

IV. BLUE TILT OF THE INFLATIONARY TENSOR FLUCTUATIONS

According to Ref. [8], an interesting feature of our model is that the spectrum for inflationary tensor fluctuations can be blue tilted if the potentials and the Gauss-Bonnet coupling functions take the form given in Eqs. (66) and (67); here and throughout this section, $\beta = 2$ is assumed. The blue tilt for inflationary tensor fluctuations is impossible to achieve in the conventional inflation models considered in Refs. [2,3] due to the monotonically decreasing Hubble rate, $\dot{H} < 0$, during slow-roll inflation. Thus, it is implies $\epsilon > 0$, and one can conclude that, from Eq. (32), the tensor spectral index for the conventional inflation models is always negative, $n_t < 0$; hence, the spectrum is called red tilted.

This situation is violated or the blue tilt for inflationary tensor mode is possible if a scalar-field climbs up its potential slope, as seen in Fig. 4, in its early evolution before rolling down. One can see from Fig. 4, particularly the blue patch, that a scalar field climbs up the potential slope if its initial value is larger than its value at which the potential takes its maximum, $\phi_0 > \phi_*$. And it simply rolls down the hill, the red patch, for $\phi_0 < \phi_*$. Therefore, we argue that the blue tilt of the spectrum for inflationary tensor modes would be realized when the scalar field is initially released at the $\phi_0 > \phi_*$ value. The spectrum would be red tilted for the scalar field that is initially released at

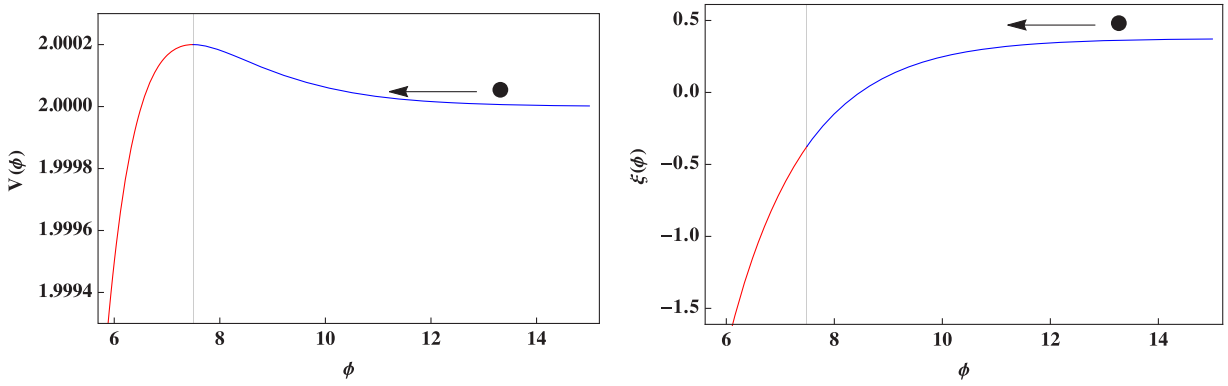

FIG. 4. Marginalized part of the potential (left) and the Gauss-Bonnet coupling (right) shown in Figs. 2(a) and 2(b) with $\alpha = 10^{-4}$. The potential energy of the scalar field takes its maximum value at ϕ_*, the vertical line. The Gauss-Bonnet coupling function $\xi(\phi)$ allows the scalar field, first, to climb up and, then, to roll down the potential slope as usual.

the $\phi_0 < \phi_*$ value. And the spectrum is scale invariant for $\phi_0 = \phi_*$.

To achieve the blue-tilted spectrum for inflationary tensor fluctuations in our model, $\epsilon < 0$ must be satisfied from Eq. (32); hence, $\dot{H} > 0$ is necessary from Eq. (7). As such, using Eq. (11) together with Eq. (15), one can easily obtain condition for Gauss-Bonnet coupling functions,

$$\xi_{,\phi} > -\frac{3}{4\kappa^4}\frac{V_{,\phi}}{V^2}, \tag{72}$$

where $V_\phi < 0$ for a scalar field which climbs up the potential slope. As long as this condition is satisfied, the blue-tilted spectrum for inflationary tensor modes would be achieved in our model. This condition is clearly satisfied for our models, and one can see that by substituting Eqs. (66) and (67) with $\beta = 2$ into Eq. (72),

$$\cosh\left(\sqrt{\frac{8\kappa^2}{q}}\phi\right)\left(\sqrt{\alpha} + \sinh\left(\sqrt{\frac{8\kappa^2}{q}}\phi\right)\right)^2 > 0, \tag{73}$$

where $\alpha > 0$ and $q > 0$. Thus, the spectrum would always be blue tilted for the potentials and the coupling functions given in Eqs. (66) and (67).

On the other hand, for successful inflation, we need about $50 \sim 60$ e-folds, or so. Therefore, it is important to know how many e-folds can be achieved so that the spectrum for the inflationary tensor mode is to be blue tilted. As we mentioned earlier, ϵ is required to be negative, from Eq. (32), for achieving the blue spectrum. And, the another criterion for the successful inflation is the smallness of the slow-roll parameter in which $|\epsilon|, |\delta_1| \ll 1$ is assumed. These conditions imply the first slow-roll parameter must take values between $-1 \ll \epsilon < 0$. After substituting Eqs. (56) and (57) into Eq. (34), we obtain

$$\epsilon = \frac{1}{\alpha + N} - \frac{N}{\alpha + N^2}, \tag{74}$$

where $\alpha > 0$. We find from Eq. (74) that the condition $-1 \ll \epsilon < 0$ is satisfied when $N > 1$. On the other hand, $\epsilon > 0$ between $0 < N < 1$; hence, the spectrum would be red tilted. In Fig. 5, we plot ϵ and n_t as a function of N.

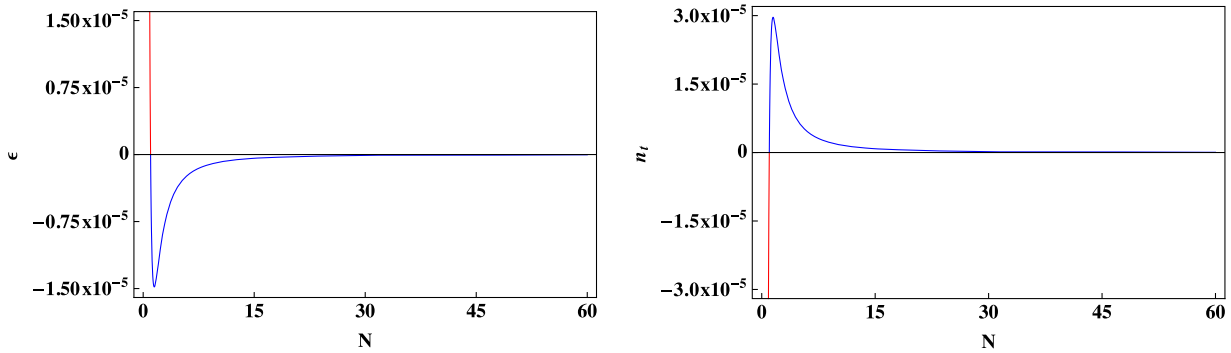

FIG. 5. $\epsilon(N)$ and $n_t(N)$ plot by using Eqs. (66) and (67). We set $\alpha = 10^{-4}$, and other numerical inputs are the same as Fig. 2. At $N = 1$, both ϵ and n_t are zero, $\epsilon = 0 = n_t$.

The red color between $0 < N < 1$ indicates positive ϵ and the red-tilted spectrum, while the blue color where $N > 1$ corresponds to negative ϵ and the blue-tilted spectrum. We conclude from Fig. 5 that for the successful inflation with a enough number of e-folds the spectrum for the primordial inflationary tensor mode would always be blue tilted.

Although δ_1 has nothing to do with the blue tilt of the inflationary tensor perturbations, it can provide constraints on the model parameters. Moreover, one can notice from Eq. (45) that the tensor-to-scalar ratio is always positive $r > 0$; hence, searching for the parameter range of δ_1 that yields $r > 0$ is necessary. We obtain $-1 \ll \delta_1 < 0$ from Eqs. (32) and (33) by assuming the smallness of the second slow-roll parameter $|\delta_1| \ll 1$. By substituting Eqs. (56) and (57) into Eq. (36), it reads

$$\delta_1 = \frac{2}{\alpha + N} - \frac{16N + q}{8(\alpha + N^2)}. \tag{75}$$

To yield the condition $-1 \ll \delta_1 < 0$, the model parameter q must take values in the ranges

$$0 < q \leq \frac{8N^3 + 8\alpha N^2 - 8\alpha N + 8\alpha^2 + 16\alpha}{\alpha + N}, \quad \text{for } N > 1, \tag{76}$$

where $\alpha > 0$. Figure 6, where we plot δ_1 and r as a functions of N, shows the validity of both $1 \ll \delta_1 < 0$ and $r > 0$. A range of q that satisfies Eq. (76) gives rise to negative δ_1 but positive r.

The most interesting and unique phenomenon for our model is that the constructed configurations of the potential and the Gauss-Bonnet coupling functions given in Eqs. (66) and (67) give rise to the blue tilt for inflationary tensor modes.

V. PROPAGATION OF THE PERTURBATIONS IN THE FRW SPACETIME

We investigated the linear perturbations about the FRW background in Sec. II. In this section, we check the stability and the ghost-free conditions in the model discussed in Sec. IV in which the blue-tilted spectrum of the inflationary tensor fluctuations is discussed. For the system to be stable, the propagation speeds for both the scalar and tensor perturbations need to be positive definite. Otherwise, the system becomes unstable; hence, a ghost appears [18–21]. From Eqs. (21), the conditions that our model have a real and nonsuperluminal propagation speed are

$$\text{Con 1}: \ 0 \leq c_s^2 = 1 - \frac{(4\epsilon + \delta_1(1 - 4\epsilon - \delta_2))\Delta^2}{4\epsilon - 2\delta_1 - 2\delta_1(2\epsilon - \delta_2) + 3\delta_1\Delta} \leq 1, \tag{77}$$

$$\text{Con 2}: \ 0 \leq c_t^2 = \frac{1 - \delta_1\delta_2}{1 - \delta_1} \leq 1. \tag{78}$$

After substituting Eqs. (66) and (67) into Eqs. (77) and (78), we plot the result in Fig. 7, and the figure shows that our model is stable by giving the positive propagation speeds, $c_s^2 \geq 0$ and $c_t^2 \geq 0$. But the condition for the subluminal propagation speed for the scalar perturbation is violated, $c_s^2 > 1$, approaching 1 from above; hence, the scalar perturbation modes propagate with speed faster than that of light, as is seen in Fig. 7(a). The propagation speed for the tensor perturbation, on the other hand, is subluminal $c_t^2 \leq 1$ according to Fig. 7(b).

Further conditions for the model to be ghost-free are discussed in Refs. [18–21] and can be written in our model from Eq. (22) as follows:

$$\text{Con 3}: \ 4\epsilon(1 - \delta_1) - \delta_1(2 - 2\delta_2 - 3\Delta) > 0, \tag{79}$$

$$\text{Con 4}: \ 1 - \delta_1 > 0. \tag{80}$$

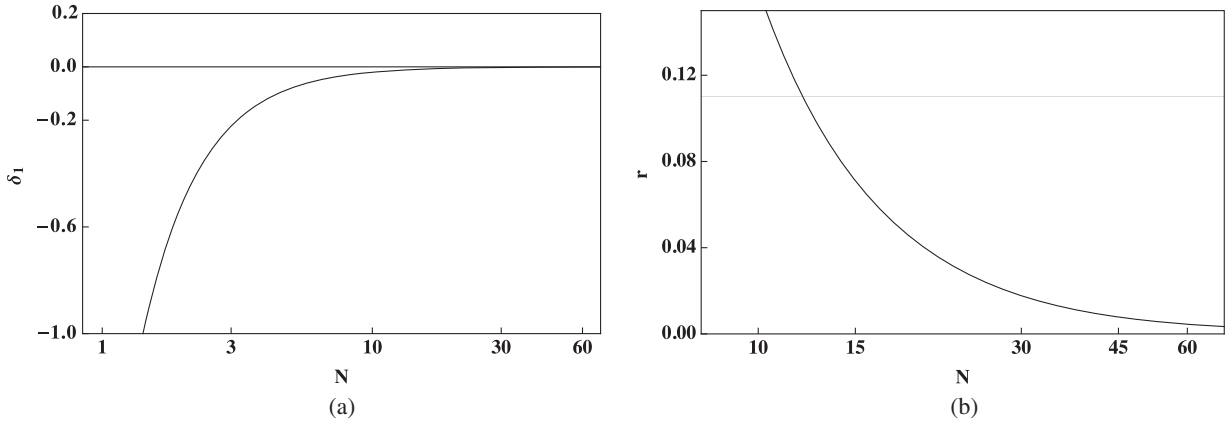

FIG. 6. $\delta_1(N)$ and $r(N)$ plot by using Eq. (66) and (67) with the same numerical inputs as Fig. 5. The horizontal line in Fig. 6(a) represents the current upper limit of the tensor-to-scalar ratio $r = 0.11$.

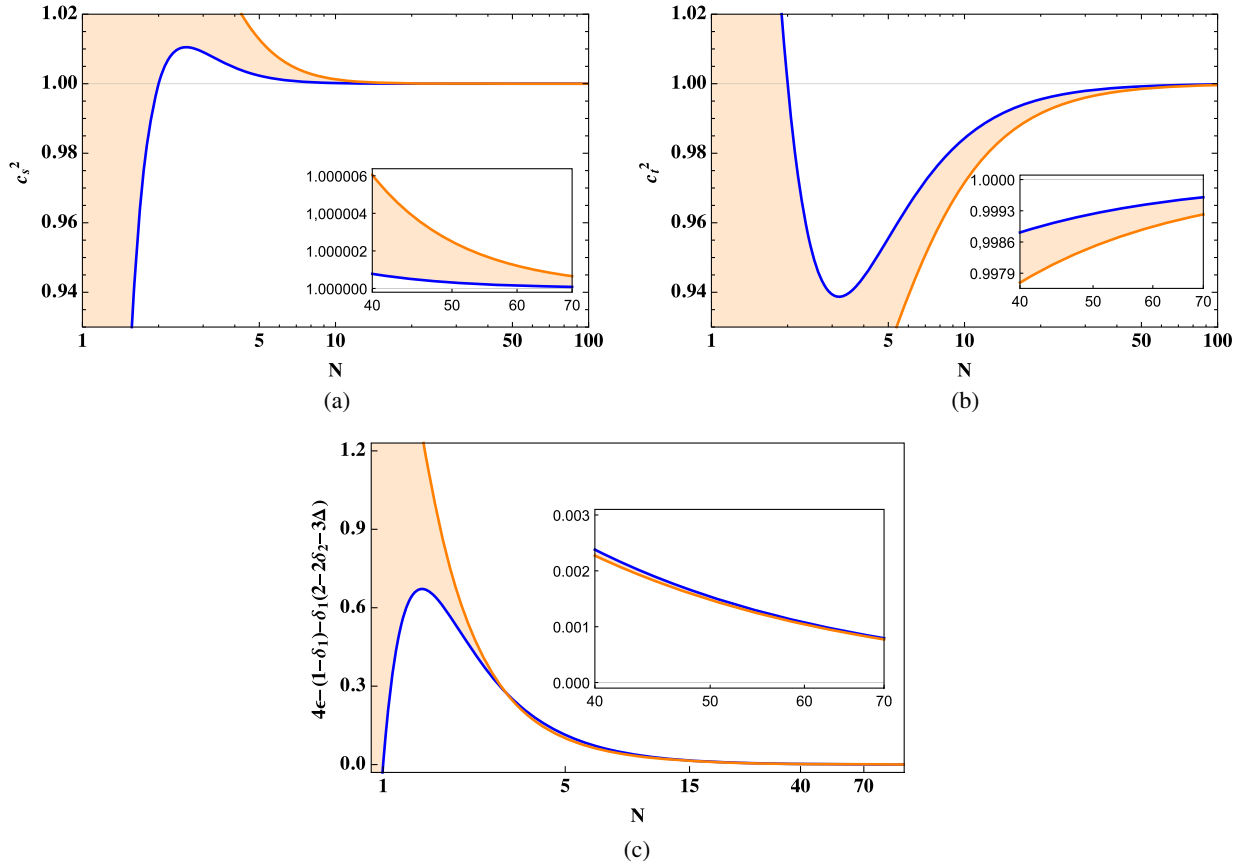

FIG. 7. The propagation speeds of both the scalar and tensor perturbations in Eqs (77) and (78) and the ghost-free condition in Eq. (79). For the shaded regions in both panels, $10^{-4} < \alpha < 1$ (from blue to orange), and other numerical inputs are the same as those used in Fig. 2.

The last condition (Con4) is clearly satisfied for our model because, from Eq. (75), $-1 \ll \delta_1 < 0$ is necessary to satisfy the smallness of the second slow-roll parameter and to yield a positive tensor-to-scalar ratio $r > 0$. Substituting Eqs. (66) and (67) into Eq. (79), we numerically show in Fig. 7(c) that the ghost-free condition is safe in our model. Thus, we conclude that the model of our interest is free of ghosts and stable. However, the propagation speed of the scalar perturbation is superluminal, while that of the tensor perturbation is subluminal.

VI. CONCLUSION

Let us conclude this work by summarizing our results; we have considered inflationary models with a Gauss-Bonnet term to reconstruct the scalar-field potentials and the Gauss-Bonnet coupling functions from the observable quantities. Assuming a specific ansatz for $n_s(N)$ and $r(N)$, as given in Eqs. (44) and (45), that are in good agreement with the observational data [2,3], the main analytic results of this work are derived in Eqs. (41) and (42).

In Sec. III, *as an exercise*, we studied the $\gamma = 1$ and $\gamma = 0$ cases of Eq. (45). The scalar-field potentials and the coupling functions for the $\gamma = 1$ case are obtained in Eqs. (51) and (52). Our result is, in this case, consistent with that of Ref. [15] when $\alpha \to 0$, in which our model reduces to the Einstein gravity where the Gauss-Bonnet term is absent or has no effect on the background evolution due to its minimal coupling to a scalar field. We then considered a $\gamma = 0$ case and reconstructed both the potentials and the coupling functions. When $p = 1$ in Eq. (45), reconstructed potentials and coupling functions in Eqs. (63) and (64) hold an inverse relation between them, and the result covers the chaotic inflation model with an inverse power-law coupling [11]. For the $p = 2$ case, we obtained the potentials and the coupling functions in Eqs. (66) and (67). The configuration of the potentials has a shape similar to a T model in Ref. [23] with a small bump on a side; see Fig. 2. The width of the potentials is characterized by the parameter q, while the height of the bump is determined by the parameter α where, if α decreases, the height of the bump decreases and eventually reduces to that of the T model. The existence of this bump on the side of the potentials implies the interesting feature of our model. Compared to the chaotic inflation with dilatonlike coupling [9] and the chaotic inflation with an inverse power-law coupling [11], the reconstructed configurations in Eqs. (66)

and (67) give rise to the observable quantities that are excellently consistent with the Planck constraints.

The key result of our work, or the most interesting feature in our model, is discussed in Sec. IV in which we considered the model with the $\gamma = 0$ and $p = 2$ case, particularly Eqs. (66) and (67) with $\beta = 2$. Our result implies that, for the reconstructed potentials and coupling functions, the blue tilt for inflationary tensor fluctuations can be realized. This blue tilt for primordial tensor modes, $n_t > 0$, is due to the fact that a scalar field climbs up its potential slope in its early stage of evolution; hence, $V_\phi < 0$ and $\epsilon < 0$. Also, to have successful inflation with a large enough number of e-folds about $50 \sim 60$, the scalar field in our model must to be released at values larger than the field value at which the potential value reached its maximum, $\phi_0 > \phi_*$. This will allow a scalar field to climb up the potential slope, and hence the spectrum would be blue tilted. Thus, in case a blue tilt for inflationary tensor fluctuation were to be detected by a future observation, that would be evidence of our model.

We also have discussed the properties of the propagating modes in the FRW background in Sec. V. Following the approaches investigated in Refs. [18–21], we have checked the ghost-free and stability conditions in our model. We found that the model, which was discussed in Sec. IV, in which the potential and the coupling functions are given in Eqs. (66) and (67), is ghost free but contains superluminal propagating scalar modes over a wide range of parameter intervals of our interest, while the tensor perturbation modes propagate with the subluminal speeds. As a future extension of the present work, we are planning to study the dynamical analysis of the system, in addition to the inflationary attractor behaviors, for the case in which the blue tilt for tensor fluctuations is realized.

ACKNOWLEDGMENTS

We appreciate Asia Pacific Center for Theoretical Physics (APCTP) for its hospitality during initiation of this work. S. K. was supported by the Basic Science Research Program through the NRF funded by the Ministry of Education (Grant No. NRF-2014R1A1A2059080). B. H. L was supported by the National Research Foundation of Korea (NRF) grant funded by the Korea government (MSIP), Grant No. 2014R1A2A1A01002306.

[1] G. Hinshaw *et al.* (WMAP Collaboration), Astrophys. J. Suppl. Ser. **208**, 19 (2013); E. Komatsu *et al.* (WMAP Collaboration), Astrophys. J. Suppl. Ser. **192**, 18 (2011); **180**, 330 (2009).
[2] P. A. R. Ade *et al.* (Planck Collaboration), Astron. Astrophys. **571**, A16 (2014); **571**, A22 (2014).
[3] arXiv:1502.01589; arXiv:1502.02114.
[4] A. H. Guth, Phys. Rev. D **23**, 347 (1981); A. Albrecht and P. J. Steinhardt, Phys. Rev. Lett. **48**, 1220 (1982); A. D. Linde, Phys. Lett. **108B**, 389 (1982).
[5] J. Martin, C. Ringeval, and V. Vennin, Phys. Dark Universe **5–6**, 75 (2014).
[6] F. L. Bezrukov and M. Shaposhnikov, Phys. Lett. B **659**, 703 (2008).
[7] A. A. Starobinsky, Phys. Lett. **91B**, 99 (1980).
[8] M. Satoh, J. Cosmol. Astropart. Phys. 11 (2010) 024.
[9] P. X. Jiang, J. W. Hu, and Z. K. Guo, Phys. Rev. D **88**, 123508 (2013).
[10] M. Satoh and J. Soda, J. Cosmol. Astropart. Phys. 09 (2008) 019.
[11] Z. K. Guo and D. J. Schwarz, Phys. Rev. D **81**, 123520 (2010).
[12] S. Koh, B. H. Lee, W. Lee, and G. Tumurtushaa, Phys. Rev. D **90**, 063527 (2014).
[13] E. J. Copeland, E. W. Kolb, A. R. Liddle, and J. E. Lidsey, Phys. Rev. D **48**, 2529 (1993).
[14] R. Easther and W. H. Kinney, Phys. Rev. D **67**, 043511 (2003); J. E. Lidsey, A. R. Liddle, E. W. Kolb, E. J. Copeland, T. Barreiro, and M. Abney, Rev. Mod. Phys. **69**, 373 (1997).
[15] T. Chiba, Prog. Theor. Exp. Phys. **2015**, 073E02 (2015).
[16] J. Lin, Q. Gao, and Y. Gong, Mon. Not. R. Astron. Soc. **459**, 4029 (2016).
[17] Y. F. Cai, J. O. Gong, S. Pi, E. N. Saridakis, and S. Y. Wu, Nucl. Phys. **B900**, 517 (2015).
[18] G. Calcagni, B. de Carlos, and A. De Felice, Nucl. Phys. **B752**, 404 (2006).
[19] A. De Felice, M. Hindmarsh, and M. Trodden, J. Cosmol. Astropart. Phys. 08 (2006) 005.
[20] J. Soda, M. a. Sakagami, and S. Kawai, arXiv:gr-qc/9807056; S. Kawai, M. a. Sakagami, and J. Soda, Phys. Lett. B **437**, 284 (1998).
[21] G. Hikmawan, J. Soda, A. Suroso, and F. P. Zen, Phys. Rev. D **93**, 068301 (2016).
[22] J. C. Hwang and H. Noh, Phys. Rev. D **71**, 063536 (2005).
[23] R. Kallosh and A. Linde, J. Cosmol. Astropart. Phys. 07 (2013) 002.